UNIVERSITY OF BIRMINGHAM

University of Birmingham Research at Birmingham

Transformation of Cs-IONSIV ® into a ceramic wasteform by hot isostatic pressing

Chen, Tzu-Yu; Maddrell, Ewan R.; Hyatt, Neil C.; Gandy, Amy S.; Stennett, Martin C.; Hriljac, Joseph A.

Document Version
Publisher's PDF, also known as Version of record

Link to publication on Research at Birmingham portal

Transformation of Cs-IONSIV® into a ceramic wasteform by hot isostatic pressing

Tzu-Yu Chen [a], Ewan R. Maddrell [b], Neil C. Hyatt [c], Amy S. Gandy [c], Martin C. Stennett [c], Joseph A. Hriljac [a], *

[a] School of Chemistry, University of Birmingham, Edgbaston, Birmingham B15 2TT, UK
[b] National Nuclear Laboratory, Workington, Cumbria CA14 3YQ, UK
[c] Department of Materials Science and Engineering, The University of Sheffield, Mappin Street, Sheffield S1 3JD, UK

HIGHLIGHTS

- A dense ceramic wasteform is prepared by hot isostatic pressing Cs-exchanged IONSIV®.
- Cs was encapsulated in two phases, $Cs_2TiNb_6O_{18}$ and $Cs_2ZrSi_6O_{15}$, in the HIPed Cs-IONSIV®.
- HIPed Cs-IONSIV® samples have low aqueous leach rates of Cs ions that are very comparable with those reported for hollandite.

ARTICLE INFO

ABSTRACT

A simple method to directly convert Cs-exchanged IONSIV® IE-911 into a ceramic wasteform by hot isostatic pressing (1100 °C/190 MPa/2 hr) is presented. Two major Cs-containing phases, $Cs_2TiNb_6O_{18}$ and $Cs_2ZrSi_6O_{15}$, and a series of mixed oxides form. The microstructure and phase assemblage of the samples as a function of Cs content were examined using XRD, XRF, SEM and TEM/EDX. The chemical aqueous durability of the materials was investigated using the MCC-1 and PCT-B standard test methods. For HIPed Cs-IONSIV® samples, the MCC-1 normalised release rates of Cs were $<1.57 \times 10^{-1}$ g m^{-2} d^{-1} at 0–28 days, and $<3.78 \times 10^{-2}$ g m^{-2} d^{-1} for PCT-B at 7 days. The low rates are indicative of a safe long-term immobilisation matrix for Cs formed directly from spent IONSIV®. It was also demonstrated that the phase formation can be altered by adding Ti metal due to a controlled redox environment.

1. Introduction

IONSIV® R9120-B Selective Media (formerly IE-911) is a commercial mixture of crystalline silicotitanate (CST) in the acid form with the formula of $(H,Na)_{2-x}(Ti_{2-x}Nb_x)SiO_7{\sim}2H_2O$ and an amorphous $Zr(OH)_4$ binder to produce a granular product suitable for engineering use. It has been widely applied in several Magnox storage ponds in the UK and various US locations including Three Mile Island, Savannah River and Oak Ridge National Laboratory as an inorganic ion exchanger [1,2]. It shows an excellent selectivity and great performance to separate ^{137}Cs and ^{90}Sr relative to Na$^+$, K$^+$ and H$^+$ from waste streams in a broad pH range [3,4]. After the severe accident at the Fukushima Daiichi nuclear power station in

2011, it has been estimated by Tokyo Electric Power Company (TEPCO) that approximately 10 PBq of ^{137}Cs released into the atmosphere [5]. IONSIV® was utilised in the Simplified Active Water Retrieve and Recovery System (SARRY) to remove caesium from the contaminated wastewater [6]. The CST sorbent contains significant quantities of titanium, which is historically difficult for processing into a wasteform via vitrification, other disposal options that have been investigated are cementation [7] and thermal conversion [8,9] to a ceramic wasteform.

To be a viable wasteform, a monolithic solid is usually preferred over a powder due to the smaller surface area, thus the release rate of any elements is reduced if the wasteform contacts water. Hot isostatic pressing (HIP) involves heating a powder sample in a sealed metal can whilst simultaneously applying pressure and it has been widely studied in the past few decades for the feasibility for nuclear waste treatment [10–17]. After HIPing, internal pores and defects within a solid are eliminated, as a consequence a

* Corresponding author.
E-mail address: j.a.hriljac@bham.ac.uk (J.A. Hriljac).

monolithic material with a uniform grain size and a nearly 100% density is achieved [18,19]. The waste to be treated is sealed in a metal can, which may also form the primary waste package containment, and processed at relatively low temperature, thus high temperature volatility losses are greatly reduced and no off-gas emission processing system is required. Furthermore, HIPing generally provides higher waste loadings than vitrification and also flexibility in handling problematic waste.

Studies of the mechanism of Cs ion selectivity in crystalline silicotitanate [20,21], the crystal structures of Cs-exchanged CST [22] and microstructure and phase transformation effected by radiation and heat [23] have been reported. To further examine the technological applicability of HIPing in Cs immobilisation, the high temperature behaviour of Cs-exchanged IONSIV® under HIPing conditions and also the chemical durability after HIPing were investigated. Preliminary aspects of this research have already been reported [9].

In addition, it is also of interest to see if hollandite, one of the titanates for hosting Cs in Synroc, can be produced during the HIPing of IONSIV® when a suitable environment is created. Hollandite has a general formula of $A_xB_yC_{8-y}O_{16}$ where $x \leq 2$, the A site is occupied by large monovalent and/or divalent cations (e.g. Cs^+ and Ba^{2+}), and the B and C sites contain octahedrally coordinated cations such as Ti^{4+} or Al^{3+} with a valence between 2 and 5. Kesson et al. [24] reported certain conditions that must be met to obtain a hollandite ceramic without forming other minor phases of poor chemical durability. Firstly, the trivalent elements must be present in sufficient quantities and the trivalent elements must not be represented by Al^{3+} alone but also by Ti^{3+}. Finally, the presence of 'reduced rutile' is also indispensable to prevent the formation of secondary phases. To test this hypothesis further HIPing studies were done with added Ti metal.

2. Experimental

2.1. Sample preparation and HIPing

Cs-exchanged IONSIV® materials were prepared by impregnating powdered IONSIV® with aqueous $CsNO_3$ at various nominal Cs loadings (0, 2, 4, 6, 8, 10 and 12 wt.%) for 3 days. The nominal loading is calculated from the mass of Cs/(mass of Cs + initial mass of IONSIV®) = 0.02, 0.04, ..., 0.12. As the exact Nb, cation and water contents of the IONSIV can vary there are some inherent errors associated with these nominal loadings. Samples were washed with DI-water and recovered by filtration, dried and calcined in air at 800 °C for 12 hrs before filling into the cans. Cs-exchanged IONSIV® samples were packed into mild steel cans with 2 mm wall thickness and hot isostatically pressed at 1100 °C and 190 MPa of argon for 2 h. Some of the 6 and 12 wt.% Cs-IONSIV® materials were also HIPed under the same condition with either 2 or 4 wt.% Ti metal powder to produce a strongly reducing environment and a source of sufficient trivalent elements (e.g. Ti^{3+}) to test if hollandite might form.

To investigate the chemical durability of the Cs phases individually, $Cs_2TiNb_6O_{18}$ and $Cs_2ZrSi_6O_{15}$ were prepared and HIPed under the same condition. The powders were synthesised via a modified aqueous precursor route reported by Balmer et al. [25] for $Cs_2ZrSi_3O_9$ synthesis. A solution was prepared by mixing 50 wt.% aqueous solution of caesium hydroxide (CsOH) with an equal volume of ethanol. 1 mL aliquots of the CsOH/ethanol solution were injected into a mixture of titanium isopropoxide/niobium ethoxide or 70 wt.% zirconium propoxide/tetraethyl orthosilicate under stirring, followed by the injection of 1 mL of ethanol. The injections of CsOH/ethanol and ethanol were repeated until the CsOH/ethanol was used up. Then an extra 2 mL of ethanol and water were added

to the mixture. The concentrations of the reactants were based on a final Cs:Ti:Nb or Cs:Zr:Si cation ratio of 2:1:6. The mixture was aged overnight and then dried in an oven at 100 °C. The precursor was then ground and pressed into pellets, these were placed in a platinum crucible and heated in air at a rate of 10 °C/min to 1200 °C and held for 15 hrs.

2.2. Characterisation

Fused borate glass beads were analysed using X-ray fluorescence spectrometry (Bruker S8 Tiger WDXRF, QUANT-EXPRESS software analysis) for elemental composition determination. Circular glass beads with flat surfaces were prepared by mixing ground samples with lithium tetraborate in a 1:10 ratio and heating in a platinum/gold crucible at 1050 °C. Ammonium iodide (NH_4I) was added to help the bead exfoliate from the crucible.

The phase assemblage of the HIPed IONSIV® samples were investigated using XRD, Rietveld refinement and scanning electron microscopy (SEM). HIPed IONSIV® samples were ground and their powder diffraction patterns were collected using laboratory (Bruker D8 Advance diffractometer operating in transmission mode using Cu $K_{\alpha1}$ radiation) and synchrotron (I11, Diamond, U.K. λ = 0.826036 Å) X-rays. Rietveld refinements of synchrotron data were performed using TOPAS 5 Academic software [26]. The starting models for each phase including lattice parameters, atomic positions, and displacement parameters were taken from the literature for ($Ti_{0.833}Nb_{0.167})O_2$ [27], $ZrSiO_4$ [28], $NaNbO_3$ [29], $ZrTiO_4$ [30], SiO_2 [31], $Cs_2TiNb_6O_{18}$ [32], and $Cs_2ZrSi_6O_{15}$ [33], respectively. For multi-phases refinements, due to the large number of variables the atomic displacement parameters were kept at default values of B_{eq} = 1.58 Å^2. Lattice parameters were optimised after the scale factors had converged and the background was graphically fitted. The peak profiles were fitted to symmetric pseudo-Voigt functions.

Weight fractions of all the phase in a multiphase system can be directly calculated by their scale factors obtained after a good pattern fitting. The relationship between the weight fraction (W_i) for each phase i and its refined scale factor (S_i) is obtained from the following equation [34].

$$W_i = \frac{S_i(ZMV)_i}{\sum_{i=0}^{n} S_i(ZMV)_i}$$

where Z is the number of formula units per unit cell, M is the unit molecular weight of the formula, and V represents unit cell volume of phase i in a mixture of n phases.

Microstructure characterisation using SEM in backscattering electron image mode on polished samples was carried out on a Philips XL30 ESEM-FEG with an Oxford Inca 300 EDS system operating at 10 kV. The microstructure of the 8 wt.% HIPed sample was also examined on a TEM (FEI Tecnai T20, operating at 200 kV) with an EDX system. The TEM sample was prepared by mechanical polishing using SiC paper and a rotating polishing wheel, followed by dimpling and ion milling using a Gatan Precision Ion Polishing System to achieve electron transparency.

2.3. Aqueous durability testing

The durability tests of monolithic and powdered HIPed IONSIV® 6 wt.% and 12 wt.% were carried out in deionised water at 90 °C, according to ASTM standard methods MCC-1 [35] and PCT-B [36]. The leachate liquid was analysed by ICP-MS (Agilent 7500ce) for element leaching. The normalised elemental leach rates were calculated as
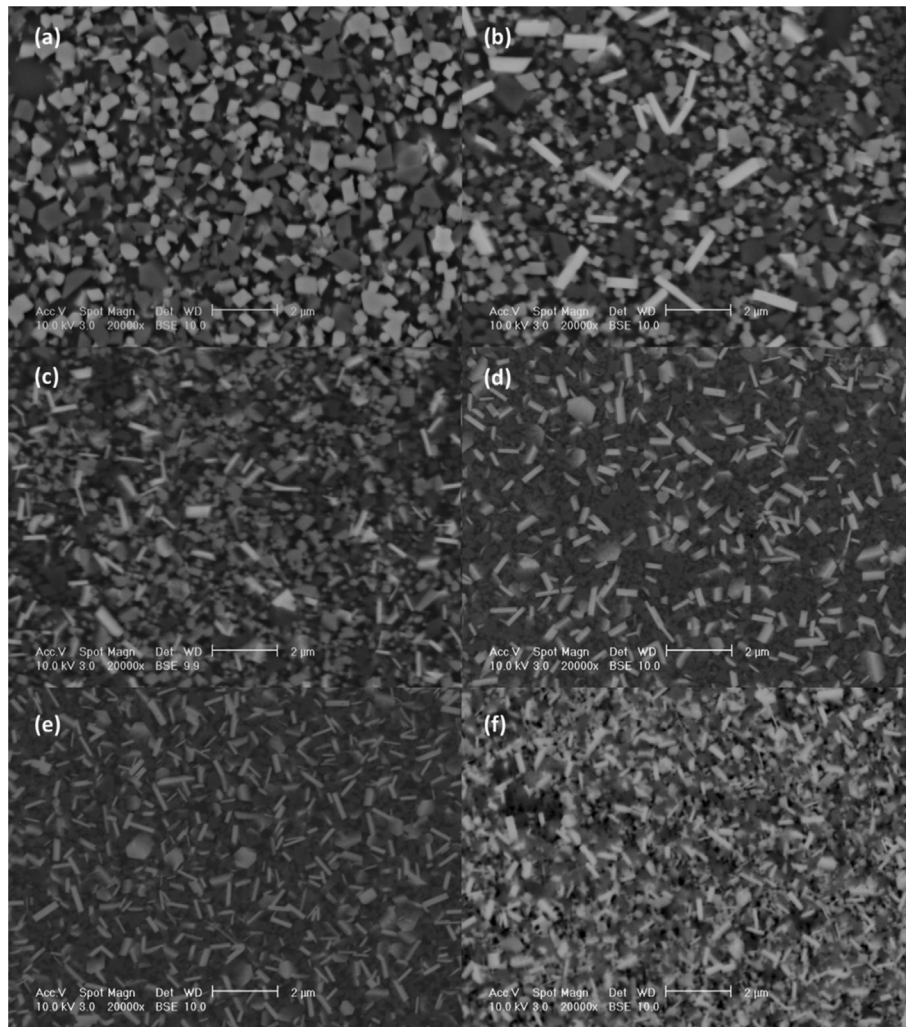
Fig. 1. The backscattering electron SEM images of HIPed (a) 2 wt.% (b) 4 wt.% (c) 6 wt.% (d) 8 wt.% (e) 10 wt.% (f) 12 wt.% Cs-IONSIV®.
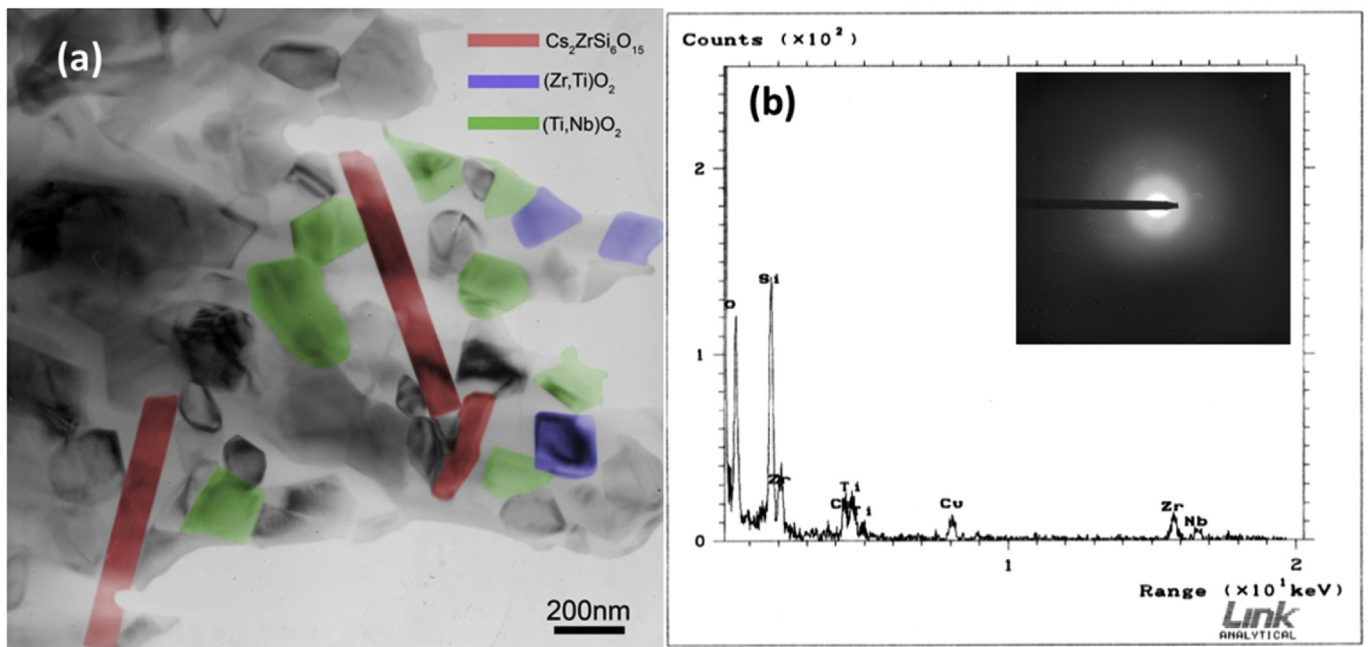

Fig. 2. TEM micrograph and diffraction pattern of the selected area in the sample of HIPed Cs-IONSIV® 8 wt.%. (a) phase map (b) amorphous silicon-rich phase detected in the other area.
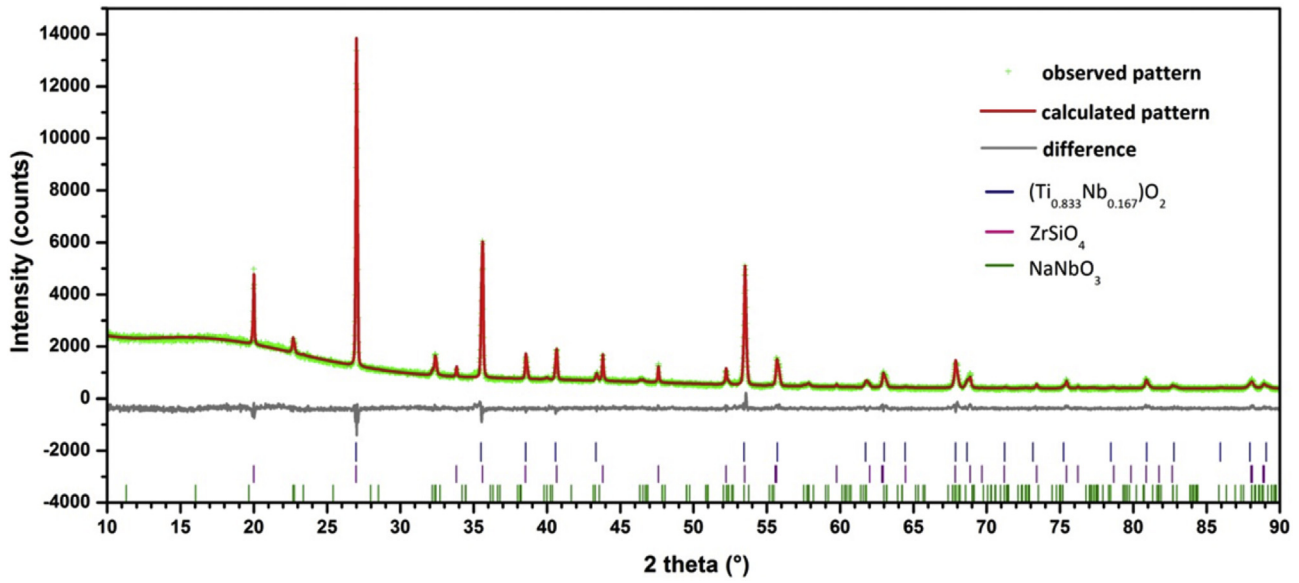
Fig. 3. Rietveld refinement fit of laboratory X-ray powder diffraction for HIPed unexchanged IONSIV®. The observed (green cross symbol), calculated (red line), and difference (grey line) profiles are shown as well as allowed positions of peaks for all phases (vertical lines). (For interpretation of the references to colour in this figure legend, the reader is referred to the web version of this article.)

Fig. 4. Synchrotron ($\lambda = 0.826036(10)$ Å) XRD patterns of HIPed (a) 2 wt.% (b) 4 wt.% (c) 6 wt.% (d) 8 wt.% (e) 10 wt.% (f) 12 wt.% Cs-IONSIV®.

$$L_i = M_i/(A_s \times t \times F_i)$$

where L_i is the leach rate (g m^{-2} d^{-1}) of element i, M_i is the mass of element i in the leachate (g), A_s is the surface area (m^2) of the sample, t is the leaching time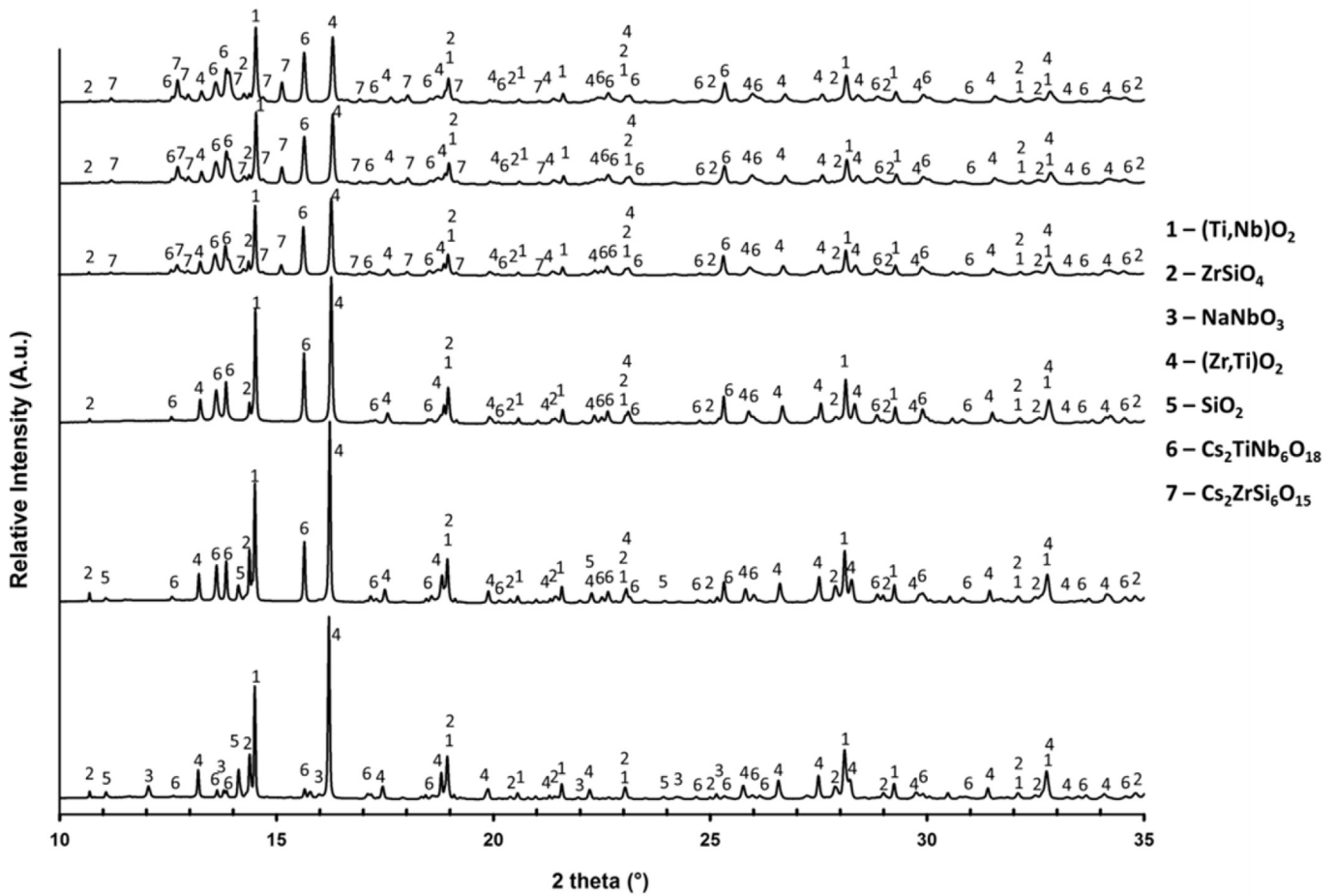 (day) and F_i is the mass fraction of element i in the original sample. The surface area used was estimated using the following equation. (see supporting information).

$$Surface\ Area = \frac{Mass\ of\ sample \times 862.2}{Theoretical\ density}$$

3. Results and discussions

3.1. Microstructure

The SEM backscattered images of HIPed Cs-IONSIV® samples with variable Cs loadings shown in Fig. 1 reveal that the microstructure of the crystalline ceramic phases reduces in grain size with an increase in Cs loading. It was also observed that more bright grains, suggesting Cs containing phases, with rectangular shape exist with the increasing Cs loading. At higher Cs content, a large number of Cs heterogeneities can act as efficient internal nucleating centres for the growth of small, randomly orientated and interlocking ceramic crystal during the heating process,
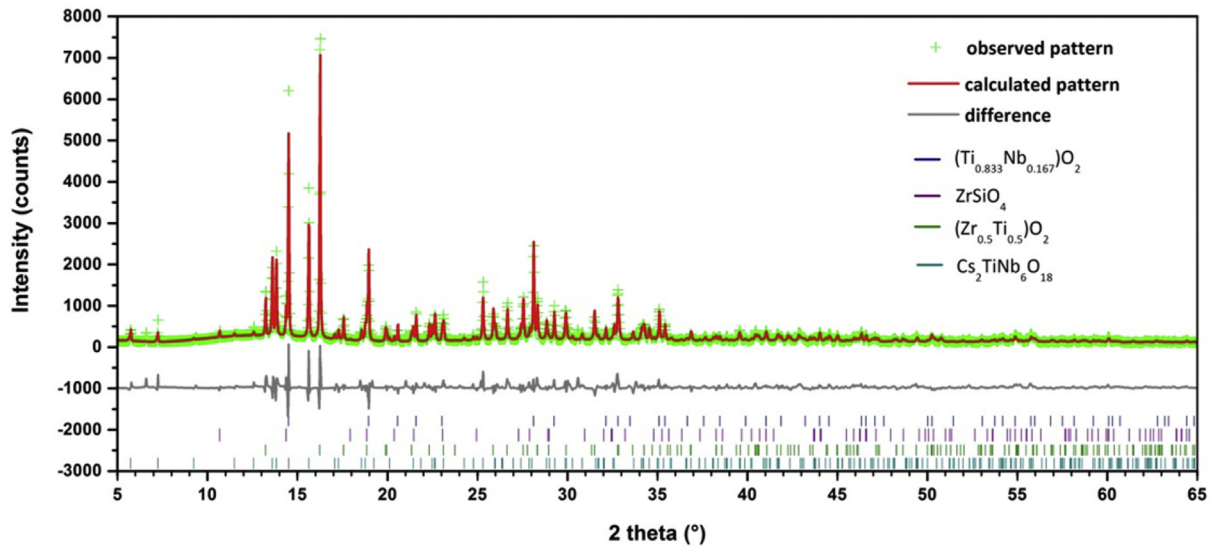
Fig. 5. Simulated (green cross symbol) and experimental diffraction patterns (red line) as well as difference pattern (grey line) and allowed positions of peaks for all phases (vertical lines) for HIPed Cs-IONSIV® 6 wt.% sample. (For interpretation of the references to colour in this figure legend, the reader is referred to the web version of this article.)
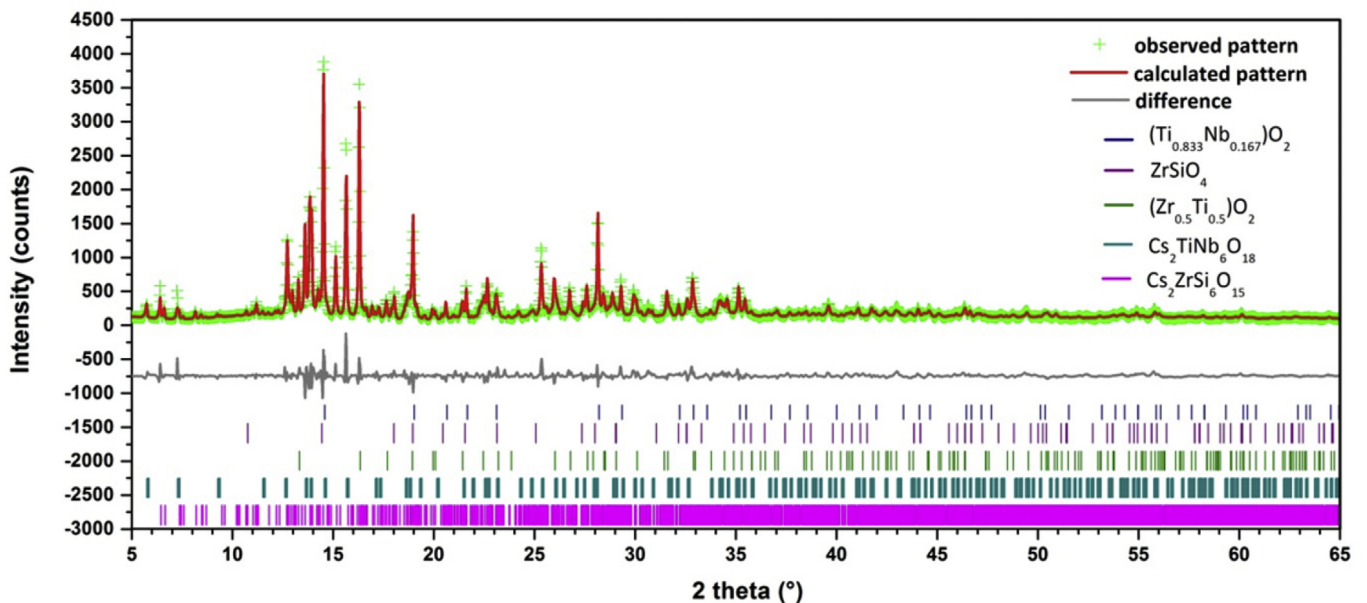
Fig. 6. Simulated (green cross symbol) and experimental diffraction patterns (red line) as well as difference pattern (grey line) and allowed positions of peaks for all phases (vertical lines) for HIPed Cs-IONSIV® 12 wt.% sample. (For interpretation of the references to colour in this figure legend, the reader is referred to the web version of this article.)
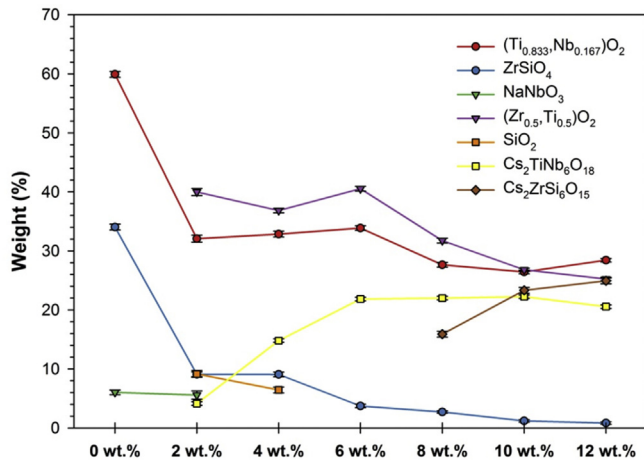
Fig. 7. The variation in the amounts of the various crystalline phases in the Cs-exchanged IONSIV® samples as a function of Cs loading.

resulting in the observed morphology with many smaller grains. However, acquiring elemental compositions of individual grains using EDS was not successful due to the inaccuracy that arose from the much larger size of the incident beam compared to the grains themselves which will excite a volume larger and deeper than a single grain.

In the bright field TEM image of HIPed 8 wt.% Cs-IONSIV® shown in Fig. 2, the identified phases are $Cs_2ZrSi_6O_{15}$, (Zr,Ti)O_2 and (Ti,Nb)O_2, confirmed using EDX. The average ratios of Zr/Ti and Ti/Nb in (Zr,Ti)O_2 and (Ti,Nb)O_2 are 5 and 1, respectively. Although $Cs_2TiNb_6O_{18}$ was not found in the region under TEM observation in Fig. 2, it was observed in other images. In addition, the EDX analysis and the corresponding diffraction pattern for a selected region in the other area confirm the presence of small amounts of an amorphous silicon-rich phase in this HIPed sample, as shown in Fig. 2b.

3.2. Phase assemblage and elemental compositions

The phase assembly of a HIPed non-exchanged IONSIV® sample was analysed using XRD and quantitative Rietveld refinement. As shown in Fig. 3, the crystalline ceramic phases consist of

Table 1
Phase assembly as a function of nominal Cs wt.% in the HIPed Cs-IONSIV® samples from refinement results and the refinement parameters.

	Cs-exchanged IONSIV® samples							Metal Ti addition	
	0 wt.%	2 wt.%	4 wt.%	6 wt.%	8 wt.%	10 wt.%	12 wt.%	2 wt.% Ti	4 wt.% Ti
(Ti$_{0.833}$Nb$_{0.167}$)O$_2$	59.9 ± 0.5%	32.1 ± 0.6%	32.9 ± 0.5%	33.9 ± 0.4%	27.7 ± 0.4%	26.4 ± 0.3%	28.4 ± 0.3%	44.6 ± 0.9%	60.9 ± 0.6%
ZrSiO$_4$	34.0 ± 0.5%	9.1 ± 0.4%	9.1 ± 0.4%	3.7 ± 0.3%	2.7 ± 0.2%	1.2 ± 0.2%	0.8 ± 0.2%	30.4 ± 0.8%	31.0 ± 0.7%
NaNbO$_3$	6.0 ± 0.4%	5.6 ± 0.7%	—	—	—	—	—	—	—
(Zr$_{0.5}$Ti$_{0.5}$)O$_2$	—	40.0 ± 0.6%	36.8 ± 0.4%	40.6 ± 0.4%	31.7 ± 0.4%	26.8 ± 0.3%	25.3 ± 0.3%	—	—
SiO$_2$	—	9.2 ± 0.6%	6.4 ± 0.5%	—	—	—	—	—	—
Cs$_2$TiNb$_6$O$_{18}$	—	4.1 ± 0.3%	14.8 ± 0.3%	21.9 ± 0.3%	22.0 ± 0.3%	22.3 ± 0.3%	20.6 ± 0.3%	—	—
Cs$_2$ZrSi$_6$O$_{15}$	—	—	—	—	15.9 ± 0.5%	23.3 ± 0.5%	24.9 ± 0.5%	25.0 ± 0.9%	—
Cs$_2$ZrSi$_3$O$_9$	—	—	—	—	—	—	—	—	31.0 ± 0.7%

Refinement parameters									
	0 wt.%	2 wt.%	4 wt.%	6 wt.%	8 wt.%	10 wt.%	12 wt.%	2 wt.% Ti	4 wt.% Ti
χ^2	1.430	3.811	3.457	2.906	2.205	2.049	2.222	2.200	1.374
R_{wp}	4.32	18.42	15.74	13.29	11.79	10.30	11.11	6.780	4.365
R_p	3.17	14.13	11.78	10.04	9.12	8.12	8.63	4.567	3.257

Table 2
Elemental composition (wt.%) of Cs-IONSIV® samples derived from the multiphase refinement of the crystalline components using laboratory XRD data for the 0 wt.% sample and synchrotron data for the others. Estimated standard deviations were calculated by propagation of the errors in the weight fractions from the Rietveld analysis.

Element	0 wt.%	2 wt.%	4 wt.%	6 wt.%	8 wt.%	10 wt.%	12 wt.%
Nb	11.4 ± 0.2	9.4 ± 0.4	11.5 ± 0.1	15.0 ± 0.1	14.3 ± 0.2	14.2 ± 0.1	13.7 ± 0.1
Zr	16.9 ± 0.2	22.5 ± 0.4	21.1 ± 0.3	20.1 ± 0.2	17.5 ± 0.2	15.4 ± 0.2	14.7 ± 0.2
Ti	20.6 ± 0.2	20.6 ± 0.3	20.6 ± 0.2	22.1 ± 0.2	17.9 ± 0.2	16.3 ± 0.1	16.6 ± 0.1
Cs	—	0.9 ± 0.1	3.4 ± 0.1	5.0 ± 0.1	10.6 ± 0.2	13.2 ± 0.2	13.4 ± 0.2
Si	5.2 ± 0.1	5.7 ± 0.3	4.4 ± 0.3	0.6 ± 0.1	3.9 ± 0.1	5.3 ± 0.1	5.6 ± 0.1
Na	0.9 ± 0.1	0.8 ± 0.1	—	—	—	—	—
O	45.0	41.2	40.2	38.4	36.8	36.5	37.0

Table 3
Elemental compositions (wt.%) of Cs-IONSIV® samples acquired using XRF, the values for oxygen are by difference to 100 wt.% rather than directly measured. Estimated standard deviations are 10% relative.

Element	0 wt.%	2 wt.%	4 wt.%	6 wt.%	8 wt.%	10 wt.%	12 wt.%
Nb	15.8 ± 1.6	15.6 ± 1.6	15.3 ± 1.5	14.8 ± 1.5	14.6 ± 1.5	14.1 ± 1.4	14.2 ± 1.4
Zr	14.3 ± 1.4	13.7 ± 1.4	13.8 ± 1.4	14.0 ± 1.4	12.9 ± 1.3	13.0 ± 1.3	13.1 ± 1.3
Ti	22.0 ± 2.2	21.3 ± 2.1	20.6 ± 2.1	19.7 ± 2.0	19.7 ± 2.0	19.2 ± 1.9	19.1 ± 1.9
Cs	—	2.7 ± 0.3	4.3 ± 0.4	7.5 ± 0.8	10.0 ± 1.0	12.0 ± 1.2	12.2 ± 1.2
Si	8.5 ± 0.9	8.4 ± 0.8	8.6 ± 0.9	8.4 ± 0.8	8.2 ± 0.8	8.0 ± 0.8	7.9 ± 0.8
Na	2.5 ± 0.3	2.1 ± 0.2	1.6 ± 0.2	0.9 ± 0.1	0.5 ± 0.1	0.2 ± 0.1	0.3 ± 0.1
O	36.9	38.9	37.4	35.6	34.6	33.7	33.5

34.0 ± 0.5 wt.% of $ZrSiO_4$, 6.0 ± 0.4 wt.% of $NaNbO_3$ and 59.9 ± 0.5 wt.% of Nb^{4+} substituted rutile-TiO_2 due to the reducing HIP condition.

Understanding the phase formation of Cs-exchanged IONSIV® under HIP conditions and the related crystallography studies of the phases is essential to reproducibly achieve the desired partitioning of Cs and predict the long-term performance of wasteforms for hosting Cs. XRD patterns of HIPed Cs-IONSIV® samples shown in Fig. 4 demonstrate the effect of Cs levels on phase assemblages. At low nominal Cs loadings, 2 to 4 wt.%, a series of oxides and a single Cs containing phase, $Cs_2TiNb_6O_{18}$, are present. A growth in intensity

of the peaks for $Cs_2TiNb_6O_{18}$ is seen with an increase of the Cs loading in the samples until about 6 wt.%, then a second Cs-containing phase, $Cs_2ZrSi_6O_{15}$, is formed and the amount of crystalline SiO_2 decreases.

To further explore the phase evolution, quantitative Rietveld refinements for weight fraction evaluation of each phase found in the samples were carried out and the results are presented in Figs. 5 to 7 and Table 1. The phase indexing was confirmed and elemental weight fractions based on the refinement results of the synchrotron data, which are shown in Table 2, generally exhibit good consistency with the elemental composition obtained from XRF, given in
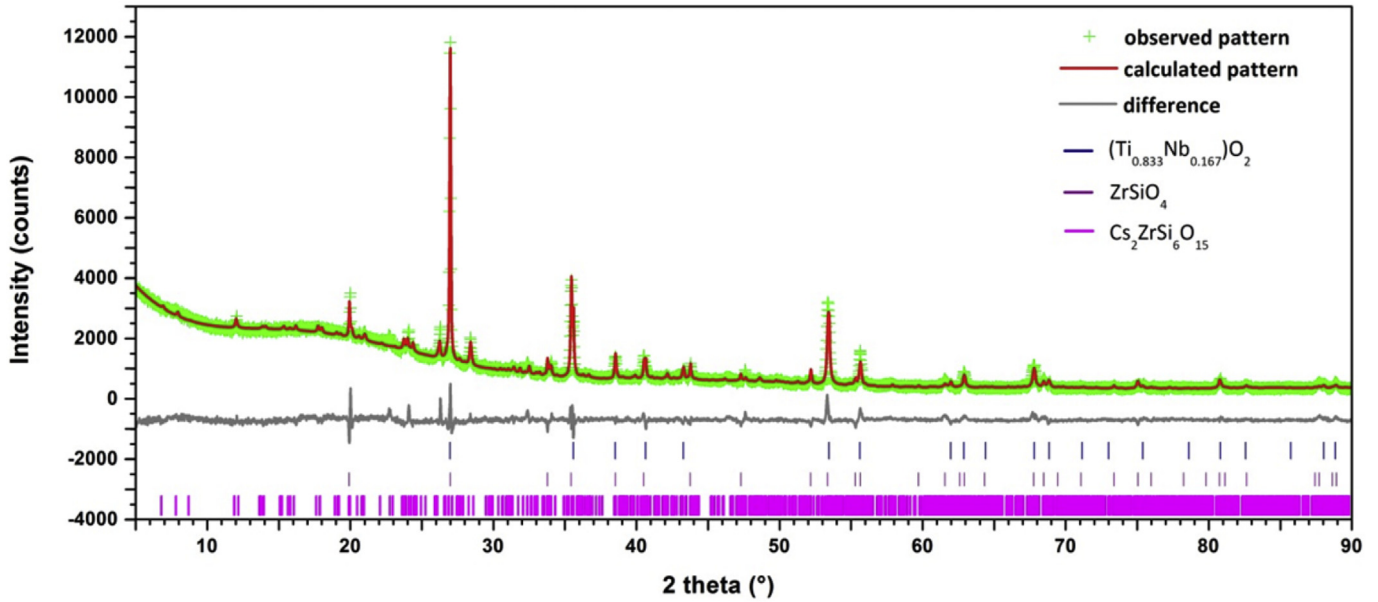

Fig. 8. Simulated (green cross) and experimental diffraction patterns (red line) as well as difference pattern (purple) and allowed positions of peaks for all phases (vertical lines) for HIPed Cs-IONSIV® 6 wt.% sample with 2 total weight percent of metallic Ti addition. (For interpretation of the references to colour in this figure legend, the reader is referred to the web version of this article.)

Fig. 9. Simulated (green cross) and experimental diffraction patterns (red line) as well as difference pattern (purple) and allowed positions of peaks for all phases (vertical lines) for HIPed Cs-IONSIV® 12 wt.% sample with 4 total weight percent of metal Ti addition. (For interpretation of the references to colour in this figure legend, the reader is referred to the web version of this article.)
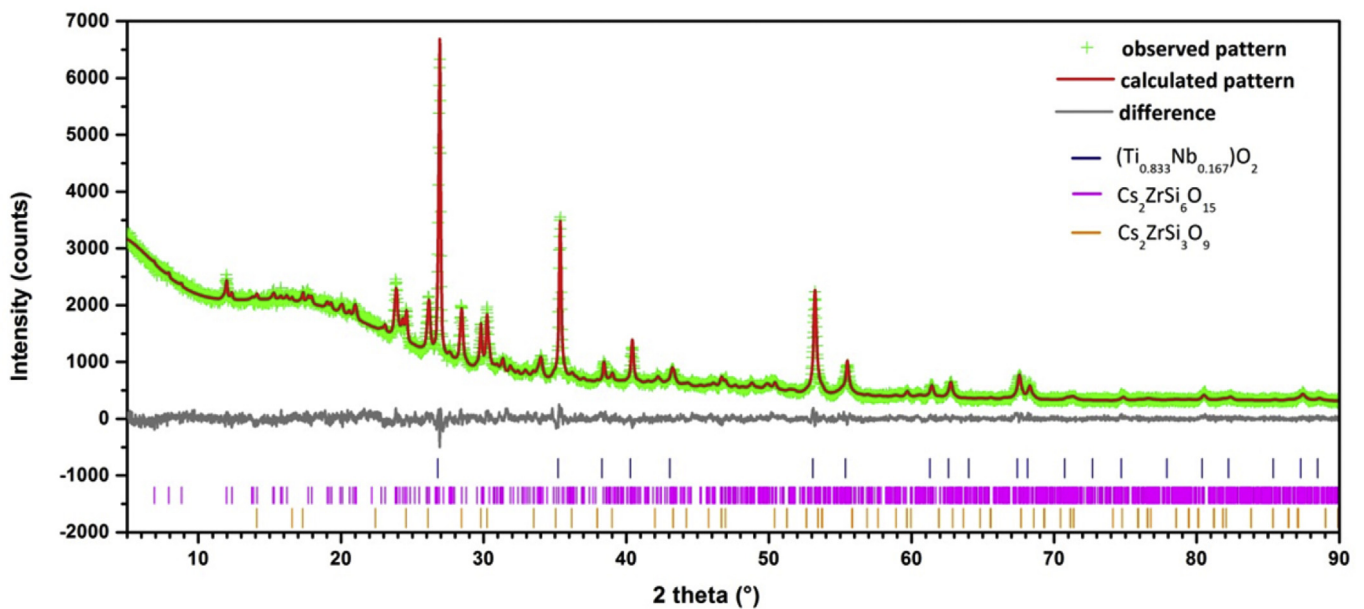
Table 3. Some of the discrepancy for Nb, Ti and Zr is likely due to fixing the Ti:Nb ratio in (Ti,Nb)O_2 to 5:1 and the Zr:Ti ratio in (Zr,Ti)O_2 to 1:1 (both averages based on TEM/EDX results from several grains in the 8 wt.% sample); due to the complexity of the XRD patterns the Nb, Ti and Zr ratios in these phases were not varied in any refinements. In addition, as noted earlier, small amounts of amorphous materials containing Si and traces of Zr and Ti were observed by TEM. The weight fractions of these amorphous substances will not be accounted for in the Rietveld analyses as an internal standard was not used. This will introduce small errors in both the derived weight fractions and elemental compositions. Importantly, both XRF and refinement results showed the weight fractions of Cs increased with the Cs loadings, as expected. The amount of $Cs_2TiNb_6O_{18}$ increases to 6 wt.% but then plateaus and $Cs_2ZrSi_6O_{15}$ forms at increased Cs loading. This appears to be due to the fact that all of the Nb becomes partitioned into $(Ti_{0.833}Nb_{0.1667})O_2$ and $Cs_2TiNb_6O_{18}$ at that point and therefore the remaining Cs must partition into the zirconium silicate, consistent with a concomittant decrease in the amount of $ZrSiO_4$. The additional missing SiO_2 is likely in glassy phases which would not be accounted for in the Rietveld refinement.

Early work by Su et al. [37] revealed that a mixture of crystalline phases appear when Cs-exchanged IONSIV® is heat-treated in air. NMR and XRD results indicated that Cs resides in a crystalline $Cs_2ZrSi_3O_9$. However, $Cs_2ZrSi_3O_9$, was not found in any of the HIPed IONSIV® samples in this work. It is suggested that a different phase formation route was created due to a more reducing environment in the HIP process than normal sintering in addition to the effect of Cs loadings.

3.3. Effect of metal additive

XRD characterisation reveals the phase assemblage in the 6 wt.% Cs-IONSIV® HIPed with 2% (total weight percentage) Ti metal addition, as shown in Fig. 8. A rutile form of (Ti,Nb)O_2, $ZrSiO_4$, and the Cs-containing phase $Cs_2ZrSi_6O_{15}$ were identified as the main phases. Quantitative phase analysis reveals that the product is comprised of 44.6 ± 0.9% of $Ti_{0.833}Nb_{0.167}O_2$, 30.4 ± 0.8% of $ZrSiO_4$ and 25.0 ± 0.9% of $Cs_2ZrSi_6O_{15}$. The absence of $Cs_2TiNb_6O_{18}$, which was found in the HIPed Cs-IONSIV® without a metal additive,
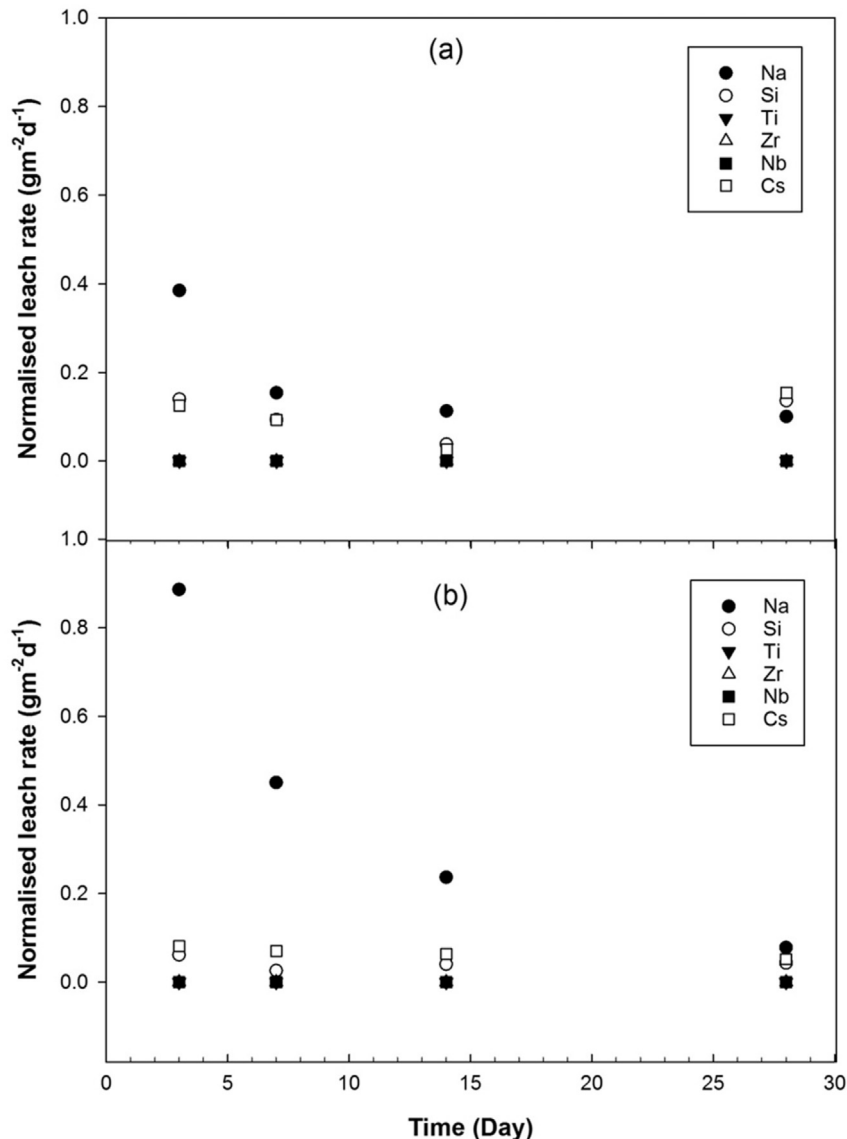
Fig. 10. Normalised leach rates from MCC-1 tests for the HIPed (a) 6 wt.% and (b) 12 wt.%. Cs-IONSIV®.

Table 4
Normalised leach rates (g m^{-2} d^{-1}) from PCT-B leach tests over 7 days for HIPed Cs-IONSIV® samples, HIPed Cs$_2$TiNb$_6$O$_{18}$ and HIPed Cs$_2$ZrSi$_6$O$_{15}$.

Element	IONSIV® 6wt.%		IONSIV® 12wt.%		Cs$_2$TiNb$_6$O$_{18}$		Cs$_2$ZrSi$_6$O$_{15}$	
	Average	Esd	Average	Esd	Average	Esd	Average	Esd
Na	0.1176	0.0166	0.1110	0.0043				
Si	0.0424	0.0036	0.0408	0.0005			0.0248	0.0004
Ti	0.0001	0.0001	0.0001	0.0001	0.0001	0.0001		
Zr	0.0005	0.0001	0.0002	0.0001			0.0004	0.0001
Nb	0.0005	0.0001	0.0001	0.0001	0.0001	<0.0001		
Cs	0.0323	0.0019	0.0378	0.0015	0.0021	<0.0001	0.0030	<0.0001

indicated that the phase transformation has been affected due to the more reducing environment; no Nb^{5+} phases (e.g. Cs$_2$TiNb$_6$O$_{18}$) form but Nb^{4+} is still found in (Ti,Nb)O$_2$. The large increase in this phase removes a significant fraction of Ti from the mixture and this is likely why no (Zr,Ti)O$_2$ is seen, the excess Zr this leaves is taken into the Cs phase and formation of a significant amount of ZrSiO$_4$. However, there is the same uncertainty in the exact Ti:Nb ratio in (Ti,Nb)O$_2$ (assumed to be 5:1) and this analysis of laboratory data suffers from significant peak overlap from that phase with ZrSiO$_4$ so the resultant weight fractions should be treated with some caution.

XRD characterisation shown in Fig. 9 reveals a slightly different phase assemblage forms in 12 wt.% Cs-IONSIV® HIPed with 4% (total weight percentage) Ti metal. With the higher Cs content and more Ti added, 60.9 ± 0.6% of Ti$_{0.833}$Nb$_{0.167}$O$_2$, 8.1 ± 0.3% of the wadeite form of Cs$_2$ZrSi$_3$O$_9$ and 31.0 ± 0.7% of Cs$_2$ZrSi$_6$O$_{15}$ were detected as main phases in the sample. No Cs$_2$TiNb$_6$O$_{18}$ was observed, as expected, and with more Cs the ZrSiO$_4$ is consumed to produce the two caesium zirconium silicates. Cs$_2$ZrSi$_6$O$_{15}$ seems to be the first Cs-containing phase to form in this Cs$_2$O-TiO$_2$-Nb$_2$O$_5$-SiO$_2$-ZrO$_2$ system under these reducing conditions and when the Si is restricted Cs$_2$ZrSi$_3$O$_9$ with a Cs:Si ratio of 2:3 forms instead of Cs:Si with a ratio of 2:6.

3.4. Aqueous durability

A systematic durability study on HIPed Cs-IONSIV® samples and the pure Cs-containing phases has been carried out using the MCC-1 and PCT-B test protocols. The MCC-1 normalised elemental leach rates of the 6 wt.% and 12 wt.% Cs-loaded HIPed IONSIV® samples against the leaching time (3, 7, 14 and 28 days) in deionised water at 90 °C are shown in Fig. 10. Both showed a relatively high but decreasing Na leach rate and almost non-leachable Ti, Nb and Zr, which is in line with PCT-B leach tests (Table 4). The Na loss is likely due to it being present in the glassy silicate phase rather than a more durable ceramic, consistent with the absence of an observed Na-containing crystalline phase in the X-ray analysis. The Cs release rates examined using both methods are not merely low but very comparable with those of HIPed Al-rich Hollandite (0.02−0.36 g m^{-2} d^{-1}) [38]. Importantly, increasing the Cs loading did not result in an increase in the normalised leach rate.

The relative stability of the phases with which these elements are associated is consistent with the dissolution nature of the wasteform. Ti and Nb, for example, are mainly related to the leaching behaviour of (Ti,Nb)O$_2$ and Cs$_2$TiNb$_6$O$_{18}$, and Zr and Si are attributed to Cs$_2$ZrSi$_6$O$_{15}$ and ZrSiO$_4$. Therefore, a Cs leaching study on the pure Cs-containing phases after HIPing, Cs$_2$TiNb$_6$O$_{18}$ and Cs$_2$ZrSi$_6$O$_{15}$, is of importance. Cs leaching experiments of HIPed Cs$_2$TiNb$_6$O$_{18}$ and Cs$_2$ZrSi$_6$O$_{15}$ were therefore carried out using MCC-1 and PCT-B standard methods and results are shown in Fig. 11 and Table 4. Based on the MCC-1 test, the HIPed 6 and 12 wt.% Cs-IONSIV® samples have essentially the same (within likely errors) Cs leach rates as either pure Cs phase from approximately 14 days. Initially the leach rate of Cs$_2$ZrSi$_6$O$_{15}$ is higher than that of

Cs$_2$TiNb$_6$O$_{18}$, but with time they appear to reach approximately the same value. We believe that the explanation for the decreasing leach rate of the zirconium phase is very much like that of a titanate hollandite where the formation of an insoluble surface oxide coating protects the bulk [39]. However, in the PCT-B test, the Cs leach rates of the HIPed IONSIV® samples are an order of magnitude higher than those of pure Cs$_2$ZrSi$_6$O$_{15}$ and Cs$_2$TiNb$_6$O$_{18}$. This is likely due to a small number of very soluble grains of a Cs-rich phase that forms during the HIP process and become exposed to the leachate in a ground sample. Indeed some amorphous Cs and Nb containing phase(s), which were not detected by XRD, were found in the HIPed 6 wt.% Cs-IONSIV® sample using SEM/EDX (see supporting information).

It is interesting to compare the chemical durability with those of other reported potential Cs wasteforms. Although the published wasteforms were produced in different ways or the conditions of the leach tests carried out were not exactly the same, the Cs retention in the HIPed Cs-IONSIV® samples and the pure Cs-containing phases is very comparable with those of Cs wasteforms such as hexagonal tungsten oxide bronze (MoW-doped HTB, MCC-1 <0.0039 g m^{-2} d^{-1} [40]), zirconium phosphates (MCC-1 ~0.01 g m^{-2} d^{-1} [41]), or pollucites (PCT 0.49 × 10^{-5} to 2.31 × 10^{-5} [42]; MCC-1 0.093 g m^{-2} d^{-1} for 28 days [16]).

It is believed that Cs$_2$TiNb$_6$O$_{18}$ exhibits good durability at least in part due to its structural features. The crystal structure of Cs$_2$TiNb$_6$O$_{18}$ (trigonal, space group $P\bar{3}m1$, $a = 7.53923(2)$ and $c = 8.19426(3)$ Å) consists of layers of (M$_6$O$_{15}$)$_n$ sheets linked by the (MO$_3$)$_n$ octahedral parallel to the c-axis by sharing corners (shown in Fig. 12a), thus cavities bounded by 21 oxygen atoms are formed. Cs cations are located between two (M$_6$O$_{15}$)$_n$ layers and almost occupy the entire volume of the "O$_{21}$"cages. The structure of
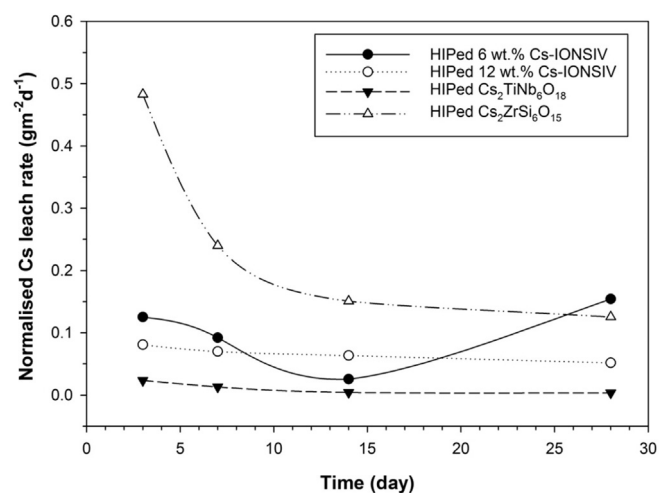
Fig. 11. Normalised Cs leach rate from MCC-1 tests for the HIPed 6 wt.% and 12 wt.%. Cs-IONSIV®, Cs$_2$TiNb$_6$O$_{18}$ and Cs$_2$ZrSi$_6$O$_{15}$.
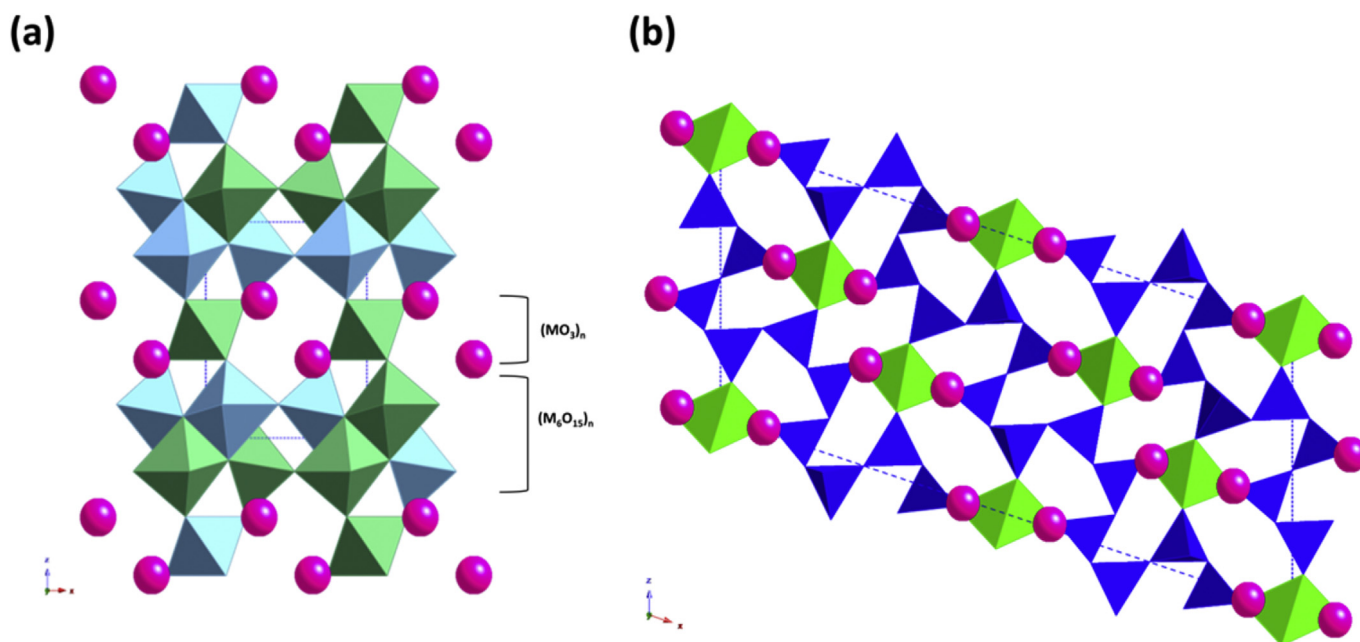
Fig. 12. (a) polyhedral (Ti/Nb) representations of $Cs_2TiNb_6O_{18}$ view along the b-axis. Blue and green octahedra correspond to two different mixed Ti/Nb sites. Pink spheres represent Cs atoms. (b) Crystal structure of $Cs_2ZrSi_6O_{15}$ as viewed down the [010] direction. Blue tetrahedra correspond to SiO_4 and green to ZrO_6 octahedra. Pink spheres represent Cs atoms. (For interpretation of the references to colour in this figure legend, the reader is referred to the web version of this article.)

$Cs_2TiNb_6O_{18}$ is rigid with no microporosity, thus the mobility of the Cs cation is limited [43,44]. A complete description of $Cs_2TiNb_6O_{18}$ structure and chemical durability can be found in our previous work [45].

Likewise Jolicart [33] has reported that the $Cs_2ZrSi_6O_{15}$ structure (monoclinic, space group $C2/m$, $a = 26.61(1)$ Å, $b = 7.506(2)$ Å and $c = 11.602(4)$ Å.) consists of connections of $Si_6O_{15}^{6-}$ sheets that are linked by ZrO_6 octahedra leaving large cavities for Cs atoms (Fig. 12b). Cs atoms are located in the cavities with 10-, 11- and 12-coordination indicating a good binding environment. The material shows low Cs release at high temperature, which accounted for diffusion pathways with no ease within the structure along which the Cs can migrate. In this work, the excellent durability in HIPed Cs-IONSIV®s, HIPed $Cs_2TiNb_6O_{18}$ and HIPed $Cs_2ZrSi_6O_{15}$ has shown that the immobilisation of Cs from IONSIV® by hot isostatic pressing is of great promise.

4. Conclusions

A durable ceramic wasteform for Cs immobilisation has been developed by direct HIPing of Cs-IONSIV® at 1100 °C/190 MPa/2 hr. XRD and Rietveld refinement results have confirmed that the Cs-IONSIV® samples were thermally decomposed and converted to two durable Cs-containing phases, $Cs_2TiNb_6O_{18}$ and $Cs_2ZrSi_6O_{15}$, and a series of mixed oxides. Cs leach rates of HIPed IONSIV® samples as well as HIPed $Cs_2TiNb_6O_{18}$ and $Cs_2ZrSi_6O_{15}$ measured using the MCC-1 and PCT-B standard tests have been carried out and compared to those of HIPed hollandite. The results showed almost no leachable Cs released from HIPed Cs-IONSIV®. Pure $Cs_2TiNb_6O_{18}$ and $Cs_2ZrSi_6O_{15}$ were also resistant to Cs leaching due to their structures.

In subsequent experiments, Ti metal has been mixed with Cs-IONSIV® and then the samples HIPed to investigate the effect of the metal additive on phase formation, with the possibility of producing hollandite-like compounds. Unfortunately, hollandite phases were never found. However, the phase assemblage has been affected due to the more reducing environment; it appears that the

redox status of the sample during HIPing was changed leading to all Nb^{5+} being reduced to Nb^{4+} to form $(Ti^{VI}, Nb^{VI})O_2$. $Cs_2TiNb_6O_{18}$ was not observed, instead the main Cs-containing phases were $Cs_2ZrSi_6O_{15}$ and $Cs_2ZrSi_3O_9$, but these are also considered potential Cs wasteforms based on the structural studies reported in the literature [25,33,46]. It also means that these Cs-containing phases can be alternative options for Cs immobilisation rather than hollandite.

HIPing provides great flexibility for producing various wasteforms such as glass, ceramic, and glass-ceramic composites that are difficult to consolidate by established methods due to factors such as high volatilisation of components/elements or low waste loading. In this work, HIPing has demonstrated to be an efficient route for densifying the materials suitable for direct and permanent disposal. More importantly, this work can provide guidance for the stabilisation of real radioactive wastes such as those generated in the cleanup efforts after the Fukushima Daiichi disaster.

accessible from the University of Birmingham Archive: http://epapers.bham.ac.uk/3042/.

Appendix A. Supplementary data

Supplementary data related to this article can be found at https://doi.org/10.1016/j.jnucmat.2017.10.011.

References

[1] F.G. Smith, S.Y. Lee, W.D. King, D.J. McCabe, Comparisons of crystalline silicotitanate and resorcinol formaldehyde media for cesium removal by in-tank column processing, Sep. Sci. Technol. 43 (2008) 2929—2942.

[2] J.F. Walker, P.A. Taylor, D.D. Lee, Cesium removal from high-pH, high-salt wastewater using crystalline silicotitanate sorbent, Sep. Sci. Technol. 34 (1999) 1167—1181.

[3] R.G. Anthony, R.G. Dosch, D. Gu, C.V. Philip, Use of silicotitanates for removing cesium and strontium from defense waste, Ind. Eng. Chem. Res. 33 (1994) 2702—2705.

[4] Z. Zheng, C.V. Philip, R.G. Anthony, J.L. Krumhansl, D.E. Trudell, J.E. Miller, Ion exchange of group I metals by hydrous crystalline silicotitanates, Ind. Eng. Chem. Res. 35 (1996) 4246—4256.

[5] Tokyo Electric Power Company, Fukushima Nuclear Accident Analysis Report, 2012.

[6] A. Holmquist, Engineered media for removal of fission products from aqueous streams, in: WM2014 Conference Proceedings, Phoenix, Arizona, USA, 2014. Phoenix, Arizona, USA, 2014.

[7] A. Jenni, N.C. Hyatt, Encapsulation of caesium-loaded Ionsiv in cement, Cem. Concr. Res. 40 (2010) 1271—1277.

[8] Y. Su, M.L. Balmer, L. Wang, B.C. Bunker, M. Nyman, T. Nenoff, A. Navrotsky, Evaluation of thermally converted silicotitanate waste forms, MRS Proc. 556 (1999) 77—84.

[9] T.-Y. Chen, J.A. Hriljac, A.S. Gandy, M.C. Stennett, N.C. Hyatt, E.R. Maddrell, Thermal conversion of Cs-exchanged IONSIV IE-911 into a novel caesium ceramic wasteform by hot isostatic pressing, MRS Proc. 1518 (2013) 67—72.

[10] Y. Zhang, M.W.A. Stewart, H. Li, M.L. Carter, E.R. Vance, S. Moricca, Zirconolite-rich titanate ceramics for immobilisation of actinides - waste form/HIP can interactions and chemical durability, J. Nucl. Mater 395 (2009) 69—74.

[11] H. Li, Y. Zhang, P.J. McGlinn, S. Moricca, B.D. Begg, E.R. Vance, Characterisation of stainless steel-synroc interactions under hot isostatic pressing (HIPing) conditions, J. Nucl. Mater 355 (2006) 136—141.

[12] S.V. Raman, Microstructures and leach rates of glass-ceramic nuclear waste forms developed by partial vitrification in a hot isostatic press, J. Mat. Sci. 33 (1998) 1887—1895.

[13] M.L. Carter, H. Li, Y. Zhang, E.R. Vance, D.R.G. Mitchell, Titanate ceramics for immobilisation of uranium-rich radioactive wastes arising from ^{99}Mo production, J. Nucl. Mater 384 (2009) 322—326.

[14] E.R. Vance, J. Davis, K. Olufson, I. Chironi, I. Karatchevtseva, I. Farnan, Candidate waste forms for immobilisation of waste chloride salt from pyroprocessing of spent nuclear fuel, J. Nucl. Mater 420 (2012) 396—404.

[15] E.R. Vance, D.S. Perera, S. Moricca, Z. Aly, B.D. Begg, Immobilisation of ^{129}I by encapsulation in tin by hot-pressing at 200°C, J. Nucl. Mater 341 (2005) 93—96.

[16] M. Omerašević, L. Matović, J. Ružić, Ž. Golubović, U. Jovanović, S. Mentus, V. Dondur, Safe trapping of cesium into pollucite structure by hot-pressing method, J. Nucl. Mater 474 (2016) 35—44.

[17] E. Maddrell, Hot isostatically pressed wasteforms for future nuclear fuel cycles, Chem. Eng. Res. Des. 91 (2013) 735—741.

[18] H.V. Atkinson, B.A. Rickinson, Hot Isostatic Processing, Adam Hilger, Bristol, 1991, p. 176.

[19] A.B. Harker, P.E.D. Morgan, J.F. Flintoff, Hot isostatic pressing of nuclear waste glasses, J. Am. Ceram. Soc. 67 (1984) C26—C28.

[20] A.J. Celestian, J.D. Kubicki, J. Hanson, A. Clearfield, J.B. Parise, The mechanism responsible for extraordinary Cs ion selectivity in crystalline silicotitanate, J. Am. Chem. Soc. 130 (2008) 11689—11694.

[21] A.J. Celestian, J.B. Parise, R.I. Smith, B.H. Toby, A. Clearfield, Role of the hydroxyl-water hydrogen-bond network in structural transitions and selectivity toward cesium in $Cs_{0.38}(D_{1.08}H_{0.54})SiTi_2O_7 \cdot (D_{0.86}H_{0.14})_2O$ crystalline silicotitanate, Inorg. Chem. 46 (2007) 1081—1089.

[22] A.J. Celestian, D.G. Medvedev, A. Tripathi, J.B. Parise, A. Clearfield, Optimizing synthesis of $Na_2Ti_2SiO_7 \cdot 2H_2O$ (Na-CST) and ion exchange pathways for $Cs_{0.4}H_{1.6}Ti_2SiO_7 \cdot H_2O$ (Cs-CST) determined from in situ synchrotron X-ray powder diffraction, Nucl. Instrum. Methods Phys. Res. Sect. B 238 (2005) 61—69.

[23] L.M. Wang, J. Chen, R.C. Ewing, Radiation and thermal effects on porous and layer structured materials as getters of radionuclides, Curr. Opin. Solid State Mat. Sci. 8 (2004) 405—418.

[24] S.E. Kesson, T.J. White, $[Ba_xCs_y][(Ti,Al)_{2x+y}Ti_{8-2x-y}]O_{16}$ synroc-type hollandites. I. Phase Chemistry, in: Proceedings of the Royal Society of London. a. Mathematical and Physical Sciences vol. 405, 1986, pp. 73—101.

[25] M.L. Balmer, Y.L. Su, H.W. Xu, E. Bitten, D. McCready, A. Navrotsky, Synthesis, structure determination, and aqueous durability of $Cs_2ZrSi_3O_9$, J. Am. Ceram. Soc. 84 (2001) 153—160.

[26] A. Coelho, TOPAS Acad. 5 (2012).

[27] M. Okrusch, R. Hock, U. Schussler, A. Brummer, M. Baier, H. Theisinger, Intergrown niobian rutile phases with Sc- and W-rich ferrocolumbite: an electron-microprobe and Rietveld study, Am. Mineral. 88 (2003) 986—995.

[28] K. Robinson, G.V. Gibbs, P.H. Ribbe, The structure of zircon: a comparison with garnet, Am. Mineral. 56 (1971) 782—790.

[29] A.W. Hewat, Neutron powder profile refinement of ferroelectric and antiferroelectric crystal structures: sodium niobate at 22°C, Ferroelectrics 7 (1974) 83—85.

[30] U. Troitzsch, A.G. Christy, D.J. Ellis, The crystal structure of disordered $(Zr,Ti)O_2$ solid solution including srilankite: evolution towards tetragonal ZrO_2 with increasing Zr, Phys. Chem. Min. 32 (2005) 504—514.

[31] K. Kihara, An X-ray study of the temperature-dependence of the quartz structure, Eur. J. Mineral. 2 (1990) 63—77.

[32] G. Desgardin, C. Robert, D. Groult, B. Raveau, New structural family - titanoniobates and titanotantalates $A_2Nb_6TiO_{18}$ and $A_2Ta_6TiO_{18}$, J. Solid State Chem. 22 (1977) 101—111.

[33] G. Jolicart, M. Leblanc, B. Morel, P. Dehaudt, S. Dubois, Hydrothermal synthesis and structure determination of $Cs_2ZrSi_6O_{15}$, Eur. J. Solid State Inorg. Chem. 33 (1996) 647—657.

[34] R.J. Hill, C.J. Howard, Quantitative phase-analysis from neutron powder diffraction data using the Rietveld method, J. Appl. Crystallogr. 20 (1987) 467—474.

[35] Standard test method for static leaching of monolithic waste forms for disposal of radioactive waste, in: ASTM International, Standard Test Method for Static Leaching of Monolithic Waste Forms for Disposal of Radioactive Waste, 1998.

[36] Standard test methods for determining chemical durability of nuclear, hazardous, and mixed waste glasses and multiphase glass ceramics: the product consistency test (PCT), in: ASTM International, Standard Test Methods for Determining Chemical Durability of Nuclear, Hazardous, and Mixed Waste Glasses and Multiphase Glass Ceramics: the Product Consistency Test (PCT) C, 2002, 1285—02.

[37] Y. Su, M.L. Balmer, L. Wang, B.C. Bunker, M. Nyman, T.M. Nenoff, A. Navrotsky, Evaluation of thermally converted silicotitanate waste forms, MRS Proc. 556 (1999). U680—U680.

[38] M.L. Carter, A.L. Gillen, K. Olufson, E.R. Vance, HIPed tailored hollandite waste forms for the immobilization of radioactive Cs and Sr, J. Am. Ceram. Soc. 92 (2009) 1112—1117.

[39] M.L. Carter, E.R. Vance, D.R.G. Mitchell, J.V. Hanna, Z. Zhang, E. Loi, Fabrication, characterization, and leach testing of hollandite, $(Ba,Cs)(Al,Ti)_2Ti_6O_{16}$, J. Mat. Res. 17 (2002) 2578—2589.

[40] V. Luca, C.S. Griffith, E. Drabarek, H. Chronis, Tungsten bronze-based nuclear waste form ceramics. Part 1. Conversion of microporous tungstates to leach resistant ceramics, J. Nucl. Mater 358 (2006) 139—150.

[41] N. Nomura, Y. Kikawada, T. Oi, Immobilization of cesium by zirconium phosphate, J. Radioanal. Nucl. Chem. 304 (2015) 683—691.

[42] Z.Z. Jing, W.B. Hao, X.J. He, J.J. Fan, Y. Zhang, J.J. Miao, F.M. Jin, A novel hydrothermal method to convert incineration ash into pollucite for the immobilization of a simulant radioactive cesium, J. Hazard. Mater 306 (2016) 220—229.

[43] G. Desgardin, C. Robert, B. Raveau, Etude du Comportement du Thallium dans de Nouvelles Structures a Tunnels Entrecroises : les Oxydes $Tl_2Nb_6TiO_{18}$ et $Tl_2Ta_6TiO_{18}$, Mat. Res. Bull. 13 (1978) 621—626.

[44] C. Robert, G. Desgardin, B. Raveau, Ion exchange properties of the oxides $Tl_2M_7O_{18}$: the oxides $(H_3O)_2M_7O_{18}$ and $A_2M_7O_{18} \cdot 2H_2O$ (A=K, Ag), J. Inorg. Nucl. Chem. 41 (1979) 893—894.

[45] T.Y. Chen, E.R. Maddrell, N.C. Hyatt, J.A. Hriljac, A potential wasteform for Cs immobilization: synthesis, structure determination, and aqueous durability of $Cs_2TiNb_6O_{18}$, Inorg. Chem. 55 (2016) 12686—12695.

[46] G.D. Ilyushin, Hydrothermal crystallization in the $CsOH-ZrO_2-SiO_2-H_2O$ and $CsCl-ZrO_2-SiO_2-H_2O$ systems at 400°C and 0.1 GPa: the structure assembly mechanism from subpolyhedral clusters for $Cs_2ZrSi_6O_{15}$ (C2/m) and $Cs_2Ti-Si_6O_{15}$ (C2/c), Russ. J. Inorg. Chem. 48 (2003) 1799—1811.